Hybrid polymer–liquid lithium ION electrolytes: Effect of carbon black during polymerization-induced phase separation

Polymer 326 (2025) 128341

Contents lists available at ScienceDirect

Polymer

journal homepage: www.elsevier.com/locate/polymer

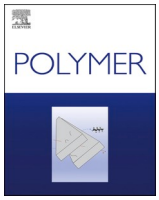

Hybrid polymer–liquid lithium ION electrolytes: Effect of carbon black during polymerization-induced phase separation

Martina Cattaruzza [a], Yuan Fang [b], István Furó [b], Göran Lindbergh [c], Fang Liu [d], Mats Johansson [a,*]

[a] Division of Coating Technology, Department of Fibre and Polymer Technology, KTH Royal Institute of Technology, SE-100 44, Stockholm, Sweden
[b] Division of Applied Physical Chemistry, Department of Chemistry, KTH Royal Institute of Technology, SE-100 44, Stockholm, Sweden
[c] Division of Applied Electrochemistry, Department of Chemical Engineering, KTH Royal Institute of Technology, SE-100 44, Stockholm, Sweden
[d] Division of Materials and Manufacture, Department of Industrial and Materials Science, Chalmers University of Technology, SE-412 96, Gothenburg, Sweden

A B S T R A C T

An increasing demand for alternative electrolyte systems is emerging to address limitations associated with traditional liquid electrolytes in lithium-ion batteries (LIBs). Hybrid polymer-liquid electrolytes (HEs) combine the merits of solid polymers and liquid electrolytes in a heterogeneous phase-separated system where the polymer phase encapsulates the liquid ion-conducting phase. These electrolytes are synthesized through polymerization-induced phase separation (PIPS), resulting in the formation of a porous three-dimensional polymer network. Carbon black (CB) serves as conductive additive in LIBs electrodes, enhancing electric conductivity and thereby improving the battery performance and lifespan. How CB, already present in conventional electrodes, affects the PIPS process during the formation of HEs for LIBs, focusing on the material interactions and the formed microstructure properties, has been investigated. Addition of CB does not negatively affect the result of PIPS process, and it permits high conversion rate and compatibility with HE at all CB concentrations investigated. Morphological analysis in combination with nuclear magnetic resonance (NMR) and electrochemical impedance spectroscopy (EIS) reveals consistent macroporous and mesoporous structures, indicating the robustness of HEs to CB content variation. Understanding the interaction between CB and HEs during the manufacturing process and the impact of CB on the structural integrity and compatibility of the HE system, aids the integration of HEs with existing electrode materials in practical battery configurations.

1. Introduction

First introduced commercially in the early 1990s, lithium-ion batteries (LIBs) have revolutionized portable electronics and electric vehicles due to their high energy density and rechargeable nature [1–3]. The overall operation of a lithium-ion battery involves the reversible transport of lithium ions between the positive electrode referred to hereafter as cathode, typically composed of metal oxides/phosphates [4] and the negative electrode referred to hereafter as anode, typically composed of carbon-based materials such as graphite [5] during charging and discharging cycles. The electrolyte is typically composed of a lithium salt dissolved in a mixture of organic solvents [6,7] and it serves as the lithium-ion-conductive medium while being electrically insulating. The core of LIBs lies in the efficient transport and reversible intercalation of lithium ions within the respective electrodes that jointly determine battery performance factors such as energy density, charging speed, lifetime and overall stability [8].

While traditional liquid electrolytes have played a crucial role in the success of LIBs [9], they pose several challenges. One significant concern is safety [10], as the flammable nature of the organic solvents in liquid electrolytes can promote thermal runaway reactions, causing fires and explosions. Moreover, the risk of leakage of liquid electrolyte due to the degradation of the battery's integrity over time can compromise performance and safety [6]. The desire for high-performance, safe, and flexible LIBs has driven research toward finding cutting-edge solutions, with a particular focus on polymer-based electrolytes [11,12] with a solid or gel-like matrix that facilitates safe and novel battery designs. This however also compromises the ionic conductivity of the system as the ion transport is slower due to increased local viscosity defined by the coordinating polymer chains [13]. Among other approaches, there is the development of hybrid polymer-liquid electrolytes (HEs), which combine the merits of liquid electrolyte systems and solid polymers. HEs typically consist of a liquid electrolyte combined with a polymer. The polymer is often cross-linked, forming a three-dimensional molecular network containing the liquid component within the macroscopic polymeric matrix, creating a gel-like structure i.e. a gel polymer electrolytes [14] (GPEs). Another possibility is the creation of a phase-separated system where the polymer and liquid components exist

* Corresponding author.
E-mail address: matskg@kth.se (M. Johansson).

https://doi.org/10.1016/j.polymer.2025.128341
Received 8 January 2025; Received in revised form 16 March 2025; Accepted 31 March 2025
Available online 1 April 2025

as distinct domains within the electrolyte. These latter electrolytes can be synthetized via a process called polymerization induced phase separation (PIPS) [15] where phase separation progresses along with the polymerization governed by the different solubilities of the monomers and the formed polymer in the liquid electrolyte. The use of PIPS as a method for creating heterogeneous electrolytes through stepwise polymerizing systems in conjunction with ionic liquids has also previously been demonstrated [16–19].

Other key components in a battery are the electrodes [20]. Additives such as polymeric binders [21] and conductive materials are incorporated into the electrode formulations of LIBs to enhance their performance [22]. The conventional manufacturing process for LIB electrodes consists of mixing the electrode components (active material, binder and conductive additive) with a solvent or a mixture of solvents to create a homogeneous slurry. The slurry is then applied to metal foils — aluminum for cathode and copper for anode — dried, and compacted to the required thickness. The electrode is eventually slit and wound before being assembled with separators and counter electrodes to form a battery cell, which is subsequently infused with the liquid electrolyte [23]. A common conductive additive to battery electrodes is carbon black (CB), typically produced via pyrolysis of either biomass or fossil sources [24], yielding fine carbon particles. A wide range of CB exist [25], most of which are nanosized, highly porous, electrically conductive particles. A typical CB used in LIBs has a particle size between 10 and 100 nm and a surface area around 50–200 m^2/g [26,27]. CB is added to cathode active materials to establish a more electrically conductive electrode by percolation which facilitates faster charge-discharge cycles. Anode active materials, although having electronic conductivity compared to cathode active materials, tend to expand and contract during charge-discharge cycles. Over time, this dimensional change causes the anode to separate, leading to the formation of 'dead' active materials which reduces the capacity of the anode after multiple cycles. There, CB is used to maintain electronic conductance and counteract this trend. Moreover, CB being porous plays a crucial role in absorbing and retaining electrolyte, facilitating close contact between lithium ions and the active materials [28]. The porous nature of CB also increases the electrode's surface area which does not facilitate Faradaic reactions but contributes to double layer charging (similar to those in a supercapacitor). However, a larger surface area can also lead to increased loss reactions, such as the formation of a solid electrolyte interphase (SEI). Electrolyte compatibility with CB particles is crucial for an optimal LIB performance. A suitable electrolyte should effectively wet the surface of CB particles, facilitating efficient ion transport during charge/discharge and leading to higher reliability and longevity of LIBs [29]. The behavior of CB under the entire process, including electrode infusion, wetting, and final structure formation, must thus be considered when introducing new electrolytes such as HEs, since CB will be present as a component in the electrode.

The influence of CB as an electrode constituent on the PIPS process when making HEs using the PIPS process has been examined. An understanding of material interactions and structural properties of the HEs in the presence of CB, which is crucial for their integration into LIBs systems, has been obtained. Studies of the PIPS process itself, as well as resulting HEs have been investigated at different CB contents. The possibility of using HEs in the manufacturing of electrodes in a more effective way compared to the presently used systems i.e. using the CB-rich HEs as conductive binder in the electrode through a one-pot process, has been presented. This could potentially mitigate the problems associated with fluorine-rich binders such as polyvinylidene fluoride (PVDF), which necessitate the use of harmful organic solvents that have significant environmental impacts [21].

2. Experimental

2.1. Materials

The commercial liquid electrolyte 1 M lithiumbis (trifuoromethanesulfonyl)imide (LiTFSI) in EC:PC 1:1 v/v, 99.9 % was purchased from Solvionic. The thermal initiator 2,2′-azobis (2-methylpropionitrile) (AIBN) was purchased from Sigma-Aldrich. The monomer bisphenol A ethoxylate dimethacrylate (BPAMA) (Mn: 540 g mol^{-1}) was provided by Sartomer (Arkema Group). CB (Super-P, TIMCAL) was purchased from Alfa Aesar (Thermo Scientific Chemicals) with a particle size of ca. 40 nm, a Brunauer-Emmett-Teller (BET) surface area = 57.0–67.0 m^2/g, and a density of 160 ± 20 kg/m^3. For the wettability test ethylene carbonate (EC), propylene carbonate (PC), and LiTFSI (99.95 % trace metal basis) were purchased from Sigma-Aldrich. All materials were utilized as received.

2.2. HE films manufacturing

A series of HEs were prepared in a glovebox under a dry argon atmosphere (<1 ppm H_2O, <1 ppm O_2). For the preparation of the HE resins, the commercial electrolyte was mixed with the monomer BPAMA, the thermal initiator AIBN and CB. The AIBN content was 1 wt % relative to the monomer weight, and the liquid electrolyte content was 45 wt % of the total weight. The samples were prepared using two different mixing methods. The first one employed the mixing of CB, whose content varied between 0 wt %, 0.5 wt %, and 0.8 wt % of the total weight, with the liquid electrolyte, and during the second stage, with the monomer. The second method increased the CB content to 1 wt % and 1.5 wt % of the total weight, mixing it first with the monomer, and in the second stage, with the liquid electrolyte. This second method allowed for higher CB contents in the resins, which would have been too viscous otherwise. Comparative analysis revealed that the microstructure and properties were consistent across both methods at these concentrations. Consequently, to avoid redundancy, results were reported only once, affirming that the two mixing approaches are comparable. The HE formulations were poured into an aluminum mold (30 × 6 × 0.5 mm^3) and subsequently covered and clamped with a glass slab. For the transversal conductivity measurements, molds designed for 15 mm diameter discs (with a thickness of 100 μm) were utilized and subsequently covered and clamped with a glass slab. Afterwards, the specimens were vacuum-sealed into a pouch bag inside the glovebox. Finally, the bagged samples were taken out of the glovebox and underwent direct thermal curing at 90 °C for 45 min in a preheated oven. Henceforth, the prepared HE samples are denoted as HE-45 wt %-xxwt % CB (with xx varying between 0 and 1.5).

2.3. Curing performance

The determination of the double bond conversion through Fourier transform infrared spectroscopy (FTIR) was conducted using a PerkinElmer Spectrum 100 instrument with a deuterated triglycine sulfate detector. The instrument was equipped with a single reflection attenuated total reflection (ATR) accessory unit, incorporating a diamond ATR crystal (Golden Gate) from Graseby Specac Ltd. Analysis of the data was performed using Spectrum software v. 10.5.1 from PerkinElmer. Two samples from each formulation were analyzed both before and after curing, with 16 scans and a resolution of 4 cm^{-1} for each spectrum. The conversion of methacrylate groups was determined by comparing the area under the vinyl peak at 1637 cm^{-1} of uncured resin and cured films. The area of the aromatic peak at 1608 cm^{-1} served as the internal reference for all spectra.

2.4. Morphology characterization

To examine the morphology and microstructure of the polymer

skeleton of HEs, broad ion beam (BIB) milling combined with scanning electron microscopy (SEM) analysis was conducted on the samples. Prior to analysis, the samples underwent a 24-h leaching in water to remove the liquid electrolyte. Subsequently, the samples were dried in a vacuum oven overnight at 60 °C. A Leica EM TIC 3X BIB was employed to produce large, finely ion-polished cross-sections of the HE for SEM analysis. A piece of HE sample (ca. 5 mm wide) was cut and glued to a Si wafer of similar size. The wafer provides a good mask for high-quality polishing on the HE. To minimize ion damage and thermal effects, the argon ion source was set at an energy of 6–6.5 kV. The finely ion-polished cross-section surfaces were analyzed using a Zeiss Ultra 55 FEG SEM equipped with a field emission electron gun. An accelerating voltage of 1 kV was employed; a working distance of 3–4 mm was used, and high-resolution images were captured using an in-lens secondary electron detector.

2.5. Percolating network formation and samples shrinkage evaluation

The assessment of the percolating polymer phase was conducted for various formulations of HEs through gravimetric analysis. Each sample underwent immersion in water (240 ml, equivalent to a water-to-sample mass ratio of 2.6) for 3 days to eliminate the liquid electrolyte (EC, PC, and LiTFSI). Subsequently, the samples were vacuum-dried at 60 °C for 3 more days. Quantification of mass loss was performed by weighing the samples before water immersion and after drying, utilizing a scale with a resolution of 0.1 mg. Four samples from each formulation were measured. The volumetric shrinkage of the different HE samples was evaluated. Each sample underwent the same treatment (leaching in water and drying) as the ones used for the aforementioned gravimetric analysis. Quantification of the volumetric shrinkage was performed by measuring the samples sizes (length, width and thickness) before water immersion and after drying, utilizing a digital slide caliper. Four samples from each formulation were measured.

2.6. Molecular and ionic mobility

In order to study the accessibility of the electrolyte species, nuclear magnetic resonance (NMR) measurements were performed using a Bruker 500 Avance III spectrometer. The HE films were cut into around 10 mm long and 3 mm wide pieces and loaded into 5 mm NMR tubes. For ^{7}Li quantification, 600 µl 1:1 w/w EC:PC was added as solvent. The $\pi/2$ pulse length is 10 µs for ^{7}Li. Not to be limited by bulk diffusion, the sample investigated was ejected, vigorously shaken and loaded into the spectrometer between measurements where one transient was recorded for each of the selected nuclei. All the measurements were conducted at 298 K.

2.7. Compatibility of CB with the HE constituents

Wettability tests of the CB particles were performed on different HE constituents in order to evaluate whether the solvents and monomer were wetting the particles. The HE constituents analyzed were the following.

- Deionized water (as not-wettable solvent reference)
- EC:PC 50:50 w/w
- 1 M LiTFSI in EC:PC 50:50 w/w
- BPAMA monomer

Around 100 mg of CB was placed in four different vials and 1 ml of each solvent was slowly added drop by drop, while closely observing the absorbance behavior. The samples were monitored for 10 min. The test was inspired by the standard ASTM D1483-12 titled “Standard Test Method for Oil Absorption of Pigments by Gardner-Coleman Method” used for determining the oil absorption rate of pigments, which is closely related to the pigment’s surface area and structure [30].

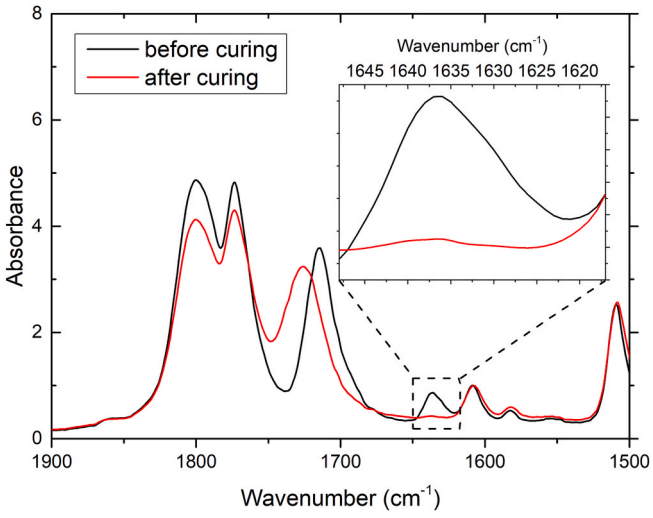

Fig. 1. FTIR spectra of the resin (before curing) and of the film (after curing) showing the disappearance of the vinyl stretch peak at 1637 cm^{-1} (see the enlarged region) for HE-45 wt %-1wt % CB.

2.8. Electrochemical performance

Electrochemical impedance spectroscopy (EIS) was employed to assess the conductivity of HEs both longitudinally (along the films lengths) and transversely (across the films thicknesses). The measurements were conducted within a glovebox immediately after preparing the respective samples to minimize the impact of solvent evaporation. The analysis of HE films conductivities was performed using a Gamry Series G 750 potentiostat/galvanostat/ZRA interface. For the longitudinal conductivity, a four-point electrode cell with gold wires serving as electrodes was used consisting of two working electrodes positioned 20 mm apart and two reference electrodes spaced 5 mm apart. For the transverse conductivity, HE discs (15 mm diameter and 100 µm thick) were sandwiched between two stainless steel blocking electrodes (15 mm diameter) in a Swagelok-type cell. Impedance measurements were carried out within the frequency range of 120 kHz to 1 Hz. The bulk resistance (R_b) was determined by identifying the low-frequency intercept on the real axis in the resulting Nyquist plot. Conductivity (σ) was then calculated using the formula $\sigma = \frac{l}{R_b * A}$ where l represents the length between the reference electrodes (5 mm for the longitudinal conductivity, ca. 100 µm for the transversal conductivity), R_b is the bulk resistance, and A is the cross-sectional area of the sample (the rectangular cross section of the film for the longitudinal conductivity, the circular area of the disc for the transversal cross section). Cross-sectional area estimations were based on measurements of thickness, width and radius using a digital slide caliper. Three samples from each formulation underwent testing.

Table 1
The average conversion of the different formulations calculated from FTIR peak intensities.

Sample	Average
HE-45 wt %-0wt % CB	96.0 ± 0.3
HE-45-wt %-0.5 wt % CB	96.6 ± 0.3
HE-45 wt %-0.8 wt % CB	96.7 ± 0.2
HE-45 wt %-1wt % CB	95.9 ± 0.1
HE-45 wt %-1.5 wt % CB	95.8 ± 0.3

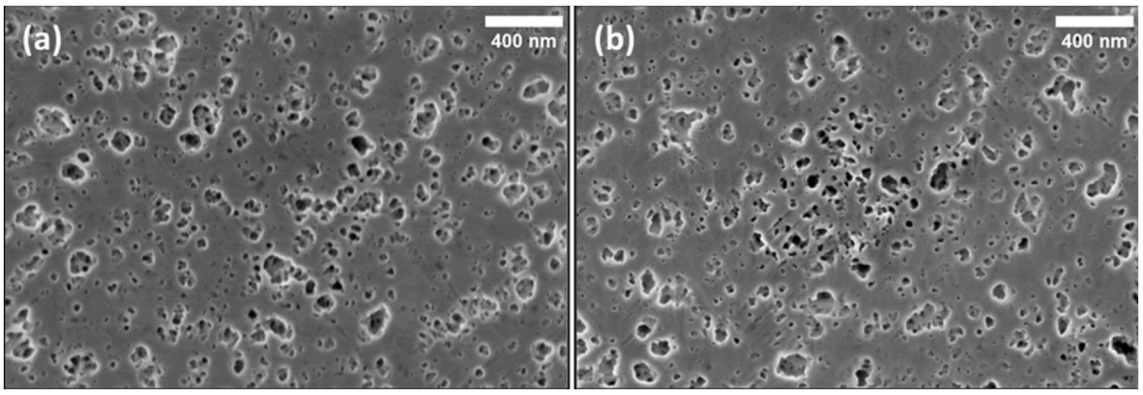

Fig. 2. SEM micrographs of BIB polished cross-section of **(a)** HE-45 wt %-0.5 wt % CB and **(b)** HE-45 wt %-1.5 wt % CB, showing similar morphology with macropores and mesopores.

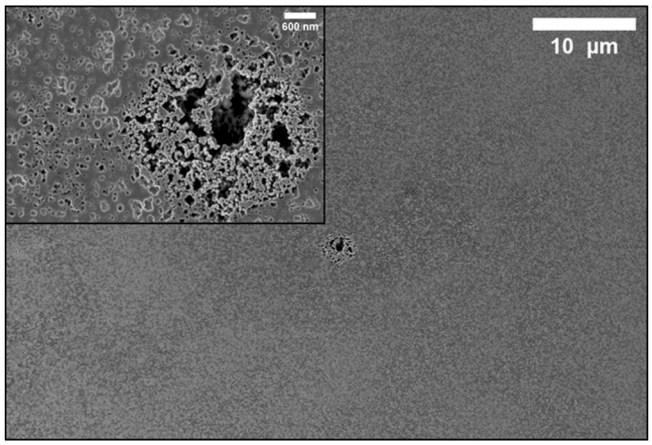

Fig. 3. SEM micrographs of BIB polished cross-section, showing inhomogeneous microstructure in HE-45 wt %-0.5 wt % CB, with an area in the centre with carbon black agglomerates. The inset shows details of the agglomerates.

3. Results and discussion

3.1. Effect of CB on PIPS reaction

Fig. 1 presents the FTIR spectra of HE-45 wt %-1wt % CB both before and after the curing process. The FTIR spectra of other formulations (Figure S1-S4) exhibit a similar trend. The disappearance of the vinyl stretch peak at 1637 cm^{-1} after curing confirms that thermal curing under the aforementioned conditions remains a reliable method for the PIPS in HE systems even when incorporating CB particles.

The quantitative FTIR findings (Table 1) indicate that a high conversion of the double bond was attained in all HE samples studied, irrespective the presence of CB particles.

3.2. Effect of CB on the obtained morphology

To overcome the limitations of conventional SEM sample preparation methods, which often create morphological artifacts on fractured surfaces [31], ion polishing on cross-sectional surfaces was employed using a BIB for the study of the different morphology of the HE formulations. The micrographs of samples HE-45 wt %-0.5 wt % CB and HE-45 wt %-1.5 wt % CB (the two extreme CB contents investigated) are illustrated in Fig. 2.

The BIB polished surfaces of all the specimens exhibit macropores and mesopores, with sizes ranging from 200 nm down to <10 nm. The morphologies of the specimens are similar to the ones studied previously by Cattaruzza et al. [32]. As evidenced in samples with the lowest and highest CB content (0.5 wt % and 1.5 wt %), no visible differences are shown when varying the CB content (intermediate CB contents shown in Figure S6-S7). Moreover, the morphologies are consistent with those without CB (Fig. S5), indicating that the presence of CB did not significantly affect the structure of the HE. It has to be noted that there are limitations of using SEM to analyse porous structures. Firstly, SEM captures images of dried samples, which deviate from the actual state of the electrolyte [31]. Secondly, the images are in two dimensions, which restricts a comprehensive understanding of the overall structure. Additionally, SEM images only represent a small portion of the specimen. In other parts of the same samples, morphological inhomogeneities are evident on the micrometer scale, primarily due to the presence of carbon black agglomerates within the HEs, as depicted in Fig. 3. Features in samples with intermediate CB content are shown in Figure S8-10.

The agglomerates to a minor extent disrupt the uniform distribution of materials, resulting in small areas that differ significantly in composition and structure, Fig. 3. The presence of such agglomerates is inevitable when CB is incorporated into a viscous initial HE resin as in the present study.

Table 2
Volumetric shrinkage and mass loss of the different samples after leaching.

Sample	Average density before leaching [mg/mm^3]	Average density after leaching [mg/mm^3]	Average Density decrease [%]	Average volumetric shrinkage [%]	Average mass loss [%]
HE-45 wt %-0wt % CB	1.21 ± 0.01	0.84 ± 0.02	30.6	22.3 ± 1.9	46.2 ± 0.4
HE-45 wt %-0.5 wt % CB	1.21 ± 0.01	0.85 ± 0.04	29.7	20.6 ± 3.6	44.3 ± 1.0
HE-45 wt %-0.8 wt % CB	1.19 ± 0.02	0.84 ± 0.03	29.1	20.4 ± 1.0	43.6 ± 0.9
HE-45 wt %-1wt % CB	1.19 ± 0.00	0.84 ± 0.03	29.4	20.9 ± 0.7	44.1 ± 1.6
HE-45 wt %-1.5 wt % CB	1.16 ± 0.01	0.82 ± 0.02	29.6	20.5 ± 1.7	44.1 ± 0.6

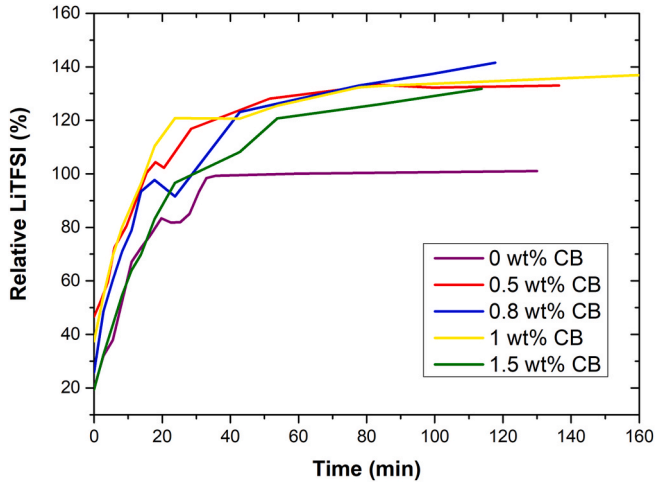

Fig. 4. Amount of LiTFSI salt released from the HEs-45 wt % with different CB content. The relative LiTFSI on the y-axis is the mass of LiTFSI relative to the nominal LiTFSI content of the HE.

Density measurements of HEs show no significant distinctions when incorporating CB into the resin (Table 2). The formulations exhibit similar densities around 1.2 mg/mm^3 before leaching and around 0.84 mg/mm^3 after leaching, indicating that CB variations within these concentrations do not significantly affect overall density. Analysis of density changes before and after leaching (and drying) reveals comparable decreases, around 30 % of the initial value. Volumetric shrinkage measurements further support this with an average volumetric shrinkage of around 21 % for all the tested formulation, consistent with results found in literature on similar samples [33]. The volume reduction observed (Table 2) can be attributable to both the shrinkage of the polymer matrix and the shrinkage of the pores due to the removal of liquid electrolytes and subsequent drying. Mass loss results in Table 2 show a complete extraction of all the liquid electrolyte phase content from the HEs for all the different formulations, demonstrating the co-existence of two phases within the system and the formation of a percolating network. The results are consistent with previous works [32]. The extracted electrolytes were all clear, colorless liquids implying that the CB is mainly within the polymer phase. The results in Table 2 indicate a consistent behavior in the HEs system, emphasizing its resilience to CB content fluctuations.

To explore the distribution of electrolytes within the different HE formulations and the correlation with conductivity values, we measured the quantities of LiTFSI present in HEs by NMR experiments. In the tests, the samples were immersed in EC:PC 50:50 w/w where ^{7}Li signal intensity was followed for determining quantitative release of LiTFSI by ^{7}Li NMR. The obtained LiTFSI release is presented in Fig. 4.

The results in Fig. 4 show that for the sample without CB, all LiTFSI was released within the first hour, as previously demonstrated [32]. For CB-containing samples the initial release amount is somewhat higher and the release rate is slightly faster. The only exception is 1.5 % CB sample which behaves similarly to the sample without. These results may indicate that there is a higher proportion of Li^+ distributed close to the surface and is perhaps related to the skin layer structure which we will discuss further in the following sections. The release is completed after the first hour. While the measured final release level differs significantly due to the sample preparations (leading to different initial lithium ion concentrations calculated as Li per HE mass), the highly similar kinetics indicates structural consistency over varying CB content.

3.3. Compatibility of constituents with CB

The compatibility of CB particles with the HEs constituents is a crucial aspect and is related to wetting that permits the electrolyte to penetrate the porous network of CB particles. A wettability test was conducted on CB particles using the different HE constituents to evaluate their wetting behavior over time. The HE constituents employed are listed in the Materials and Methods section. Deionized water, known for its high surface tension and used in this study only as a non-wettable reference for CB, formed distinct droplets on the particles' surface (Figs. S11–a), confirming the expected non wettable characteristics. In contrast, EC:PC 50:50 w/w demonstrated wettable behavior, spreading uniformly across the particles surface (Figs. S11–b). Similarly, the presence of 1 M LiTFSI in EC:PC 50:50 w/w enhanced wetting, indicating improved interaction between the solvent and CB (Figs. S11–c). Lastly, BPAMA also exhibited good wetting behavior on CB particles although the resin diffusion within the particles was slower due to the higher viscosity (Figs. S11–d).

It is important to note that the wettability and penetration of the HE constituent liquids into CB is a critical aspect of this study. While measuring wetting in a highly porous materials is generally challenging, the present wettability test is a straightforward visual assessment of liquid imbibition designed to verify expected behaviors [34] where non-polar organic substances clearly demonstrate wetting and penetration, whereas water clearly does not.

Table 3
Longitudinal conductivity and transversal conductivity results from the EIS measurement.

Sample	Longitudinal Average Conductivity [10^{-4} S*cm^{-1}]	Transversal Average Conductivity [10^{-4} S*cm^{-1}]
HE-45 wt %-0wt % CB	1.4 ± 0.1	2.3 ± 0.1
HE-45 wt %-0.5 wt % CB	2.3 ± 0.2	0.4 ± 0.3
HE-45 wt %-0.8 wt % CB	3.3 ± 0.6	0.2 ± 0.1
HE-45 wt %-1wt% CB	4.8 ± 0.3	0.3 ± 0.2
HE-45 wt%-1.5 wt% CB	21 ± 8	0.2 ± 0.1

3.4. Effect of CB on HE conductivity

The EIS results (Table 3) reveal a noticeable increase in conductivity with increasing CB content.

The presence of CB is known to facilitate efficient charge/discharge processes by forming an electron-conducting network within the electrode. When CB is added to viscous HE resins like in the present study, it is difficult to obtain an even distribution of the CB particles. As a consequence, there is the risk of aggregation of CB particles that forms conductive domains like the ones shown in Fig. 3 and Figure S8-S10. Since the pore morphology, primarily determining the ionic conductivity, seems to be constant, it is likely that the order-of-magnitude increase in conductivity is connected to an increasing electronic conductivity over a percolating CB network. Yet, it has been previously demonstrated that a deliberate addition of electronically conductive carbon filler within a determined percolating threshold can, under suitable conditions, significantly enhance even the ionic conductivity of solid-polymer electrolytes [35].

Generally, electronic conduction in battery electrolytes on a full cell level is undesirable as it can result in electron leakage or energy loss. Specifically, if electrons are able to freely move through the electrolyte, they might bypass the intended electrochemical pathways of the battery, leading directly to the opposite electrode without contributing to the battery's energy storage process. Moreover, such leakage could potentially lead to other issues like self-discharge or even short-circuiting. On the other hand, electronic conduction in CB-influenced HE within the electrode region can be advantageous. In the present system, further

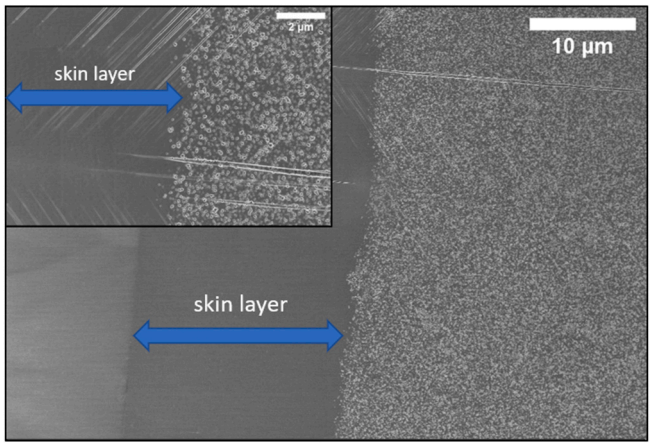

Fig. 5. SEM micrographs of BIB polished cross-section of sample HE-45 wt %-0.5 wt % CB showing the surface skin layer at the edges of the specimen. The inset is at a higher magnification.

measurements are required to ascertain whether the CB particles and their agglomerates in the HE also affect the measured conductivity by improving ion conductivity.

3.5. Skin layer formation

The manufacturing process of HEs samples can significantly impact the isotropy of electrochemical properties, potentially introducing variations in conductivity along different axes due to particle distribution and interface morphology. In order to better understand the isotropy of the conductivity in the HEs samples, the transversal conductivity across the samples thicknesses was measured. Table 3 presents a summary of the transversal conductivity values for the different HE formulations. The results show a significant decrease of the transversal conductivity when compared with the longitudinal one. The EIS setup was rigorously tested to ensure that it did not introduce any inherent resistive elements. The results show an average transversal resistance of 1.7 Ω and thereby guaranteeing the reliability of the measured conductivities in the studied HE formulations. We ascribe the decrease in conductivity in the transversal direction to the formation of a surface skin layer, as suggested by the cross-section SEM images (Fig. 5). The images reveal a solid polymer matrix without pores or particles at the edges of the HE-45 wt %-0.5 wt % CB sample.

In order to mitigate the formation of surface skin layer, the liquid electrolyte phase content was increased to 50 wt % (in a sample with 0.5 wt % CB). In certain regions of the sample, successful removal of the skin layer was achieved (Fig. 6a), while a much thinner skin layer was observed in other regions (Fig. 6b). However, varying the CB content does not influence the skin layer formation.

While the exact cause of the skin layer formation remains a subject of further investigation, one plausible explanation is linked to the manufacturing process of the HE films [36]. The interplay between the surface tensions of the HEs constituents at the interface and the processing conditions are plausible factors affecting this. Related research has being conducted on the suppression of the surface skin layer in freestanding monolithic membranes in the field of lithium ion batteries separators [37]. An in-depth exploration of this phenomenon will be instrumental in not only unraveling the origin of the surface skin layer formation but also in developing strategies to control and manipulate the properties of HEs for enhanced electrochemical performance.

4. Conclusion

The compatibility and structural influence of CB on HEs during the PIPS process, which is critical for the development of HEs in advanced battery systems, has been highlighted. Valuable insights for future assessments of the electrochemical performance of HEs in practical battery configurations, such as those with commercial electrodes, have been provided. The results clearly demonstrated that CB integrates with HE both with respect to the HE formation (PIPS) and the HE overall final performance. The chemical conversion as well as the phase separation process was unaffected by the presence of CB up to 1.5 wt %. This was further supported by SEM images, which showed consistent macroporous and mesoporous structures in all formulations, irrespective of CB content. NMR and leaching tests showed that a fully percolating system was obtained for all the samples analyzed. The introduction of CB in varying concentrations enhances conductivity in HEs up to one order of magnitude increase with 1.5 wt % CB content, indicating a concentration-dependent relationship and emphasizing CB's role in optimizing the electrochemical performance. The results confirm the findings from previous work on HEs and their interactions with commercial cathodes, where it was proven that the presence of active material constituents during polymerization does not alter the microstructural morphology or the electrochemical behavior of the HEs [38]. Furthermore, the CB integration primarily occur within the polymer phase, supporting its potential role as an electronic conductor in composite electrodes. These insights reinforce the feasibility of using HEs as both electrolyte and binder, paving the way for an innovative method that potentially streamlines LIB electrode production using a one-pot process.

CRediT authorship contribution statement

Martina Cattaruzza: Writing – review & editing, Writing – original draft, Visualization, Validation, Software, Project administration, Methodology, Investigation, Formal analysis, Data curation, Conceptualization. **Yuan Fang:** Writing – original draft, Methodology, Formal

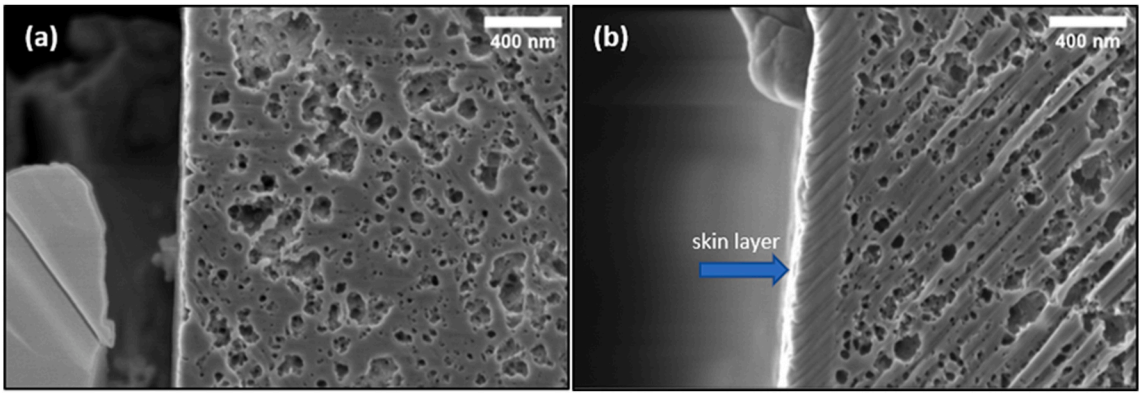

Fig. 6. SEM micrographs of BIB polished cross-section of sample HE-50 wt %-0.5 wt % CB: **(a)** region without and **(b)** region with a thin surface skin layer.

analysis, Data curation. **István Furó:** Writing – review & editing, Writing – original draft, Supervision, Resources, Funding acquisition. **Göran Lindbergh:** Writing – review & editing, Writing – original draft, Supervision, Resources. **Fang Liu:** Writing – review & editing, Writing – original draft, Supervision, Resources, Methodology, Formal analysis. **Mats Johansson:** Writing – review & editing, Writing – original draft, Supervision, Resources, Funding acquisition.

Declaration of competing interest

The authors declare that they have no known competing financial interests or personal relationships that could have appeared to influence the work reported in this paper.

Acknowledgements

The Swedish Energy Agency (grant #48488, P2023-00097) and the Swedish Research Council VR are gratefully acknowledged for financial support.

Appendix A. Supplementary data

Supplementary data to this article can be found online at https://doi.org/10.1016/j.polymer.2025.128341.

Data availability

Data will be made available on request.

References

[1] M. Armand, P. Axmann, D. Bresser, M. Copley, K. Edström, C. Ekberg, D. Guyomard, B. Lestriez, P. Novák, M. Petranikova, W. Porcher, S. Trabesinger, M. Wohlfahrt-Mehrens, H. Zhang, Lithium-ion batteries – current state of the art and anticipated developments, J. Power Sources 479 (2020).
[2] J. Xu, X. Cai, S. Cai, Y. Shao, C. Hu, S. Lu, S. Ding, High-energy lithium-ion batteries: recent progress and a promising future in applications, EEM 6 (5) (2023).
[3] M. Armand, J.M. Tarascon, Building better batteries, Nat 451 (7179) (2008) 652–657.
[4] W. Lee, S. Muhammad, C. Sergey, H. Lee, J. Yoon, Y.M. Kang, W.S. Yoon, Advances in the cathode materials for lithium rechargeable batteries, Angew Chem. Int. Ed. Engl. 59 (7) (2020) 2578–2605.
[5] S. Li, K. Wang, G. Zhang, S. Li, Y. Xu, X. Zhang, X. Zhang, S. Zheng, X. Sun, Y. Ma, Fast charging anode materials for lithium-ion batteries: current status and perspectives, Adv. Funct. Mater. 32 (23) (2022).
[6] J. Kalhoff, G.G. Eshetu, D. Bresser, S. Passerini, Safer electrolytes for lithium-ion batteries: state of the art and perspectives, ChemSusChem 8 (13) (2015) 2154–2175.
[7] M. Yuan, K. Liu, Rational design on separators and liquid electrolytes for safer lithium-ion batteries, J. Energy Chem. 43 (2020) 58–70.
[8] K.W. Beard, Linden's Handbook of Batteries, fifth ed., McGraw Hill LLC, 2019.
[9] E. Quartarone, P. Mustarelli, Review—emerging trends in the design of electrolytes for lithium and post-lithium batteries, JES (J. Environ. Sci.) 167 (5) (2020).
[10] M. Piglowska, B. Kurc, M. Galinski, P. Fuc, M. Kaminska, N. Szymlet, P. Daszkiewicz, Challenges for safe electrolytes applied in lithium-ion cells-A review, Mater 14 (22) (2021) 6783.
[11] D. Zhou, D. Shanmukaraj, A. Tkacheva, M. Armand, G. Wang, Polymer electrolytes for lithium-based batteries: advances and prospects, Chem 5 (9) (2019) 2326–2352.
[12] A. Arya, A.L. Sharma, Polymer electrolytes for lithium ion batteries: a critical study, Ionics 23 (3) (2017) 497–540.
[13] J. Chattopadhyay, T.S. Pathak, D.M.F. Santos, Applications of polymer electrolytes in lithium-ion batteries: a review, Polymers 15 (19) (2023) 3907.
[14] M. Zhu, J. Wu, Y. Wang, M. Song, L. Long, S.H. Siyal, X. Yang, G. Sui, Recent advances in gel polymer electrolyte for high-performance lithium batteries, J. Energy Chem. 37 (2019) 126–142.
[15] N. Ihrner, W. Johannisson, F. Sieland, D. Zenkert, M. Johansson, Structural lithium ion battery electrolytes *via* reaction induced phase-separation, J. Mater. Chem. A 5 (48) (2017) 25652–25659.
[16] M.W. Schulze, L.D. McIntosh, M.A. Hillmyer, T.P. Lodge, High-modulus, high-conductivity nanostructured polymer electrolyte membranes via polymerization-induced phase separation, Nano Lett. 14 (1) (2014) 122–126.
[17] S.A. Chopade, J.G. Au, Z. Li, P.W. Schmidt, M.A. Hillmyer, T.P. Lodge, Robust polymer electrolyte membranes with high ambient-temperature lithium-ion conductivity via polymerization-induced microphase separation, ACS Appl. Mater. Interfaces 9 (17) (2017) 14561–14565.
[18] S.A. Chopade, S. So, M.A. Hillmyer, T.P. Lodge, Anhydrous proton conducting polymer electrolyte membranes via polymerization-induced microphase separation, ACS Appl. Mater. Interfaces 8 (9) (2016) 6200–6210.
[19] L.D. McIntosh, M.W. Schulze, M.T. Irwin, M.A. Hillmyer, T.P. Lodge, Evolution of morphology, modulus, and conductivity in polymer electrolytes prepared via polymerization-induced phase separation, Macromolecules (Washington, DC, U. S.) 48 (5) (2015) 1418–1428.
[20] J.P. Pender, G. Jha, D.H. Youn, J.M. Ziegler, I. Andoni, E.J. Choi, A. Heller, B. S. Dunn, P.S. Weiss, R.M. Penner, C.B. Mullins, Electrode degradation in lithium-ion batteries, ACS Nano 14 (2) (2020) 1243–1295.
[21] B. Chen, Z. Zhang, M. Xiao, S. Wang, S. Huang, D. Han, Y. Meng, Polymeric binders used in lithium ion batteries: actualities, strategies and trends, Chemelectrochem (2024) e202300651 n/a (n/a).
[22] A.M. Haregewoin, A.S. Wotango, B.-J. Hwang, Electrolyte additives for lithium ion battery electrodes: progress and perspectives, Energy Environ. Sci. 9 (6) (2016) 1955–1988.
[23] W.B. Hawley, J. Li, Electrode manufacturing for lithium-ion batteries—analysis of current and next generation processing, J. Energy Storage 25 (2019) 100862.
[24] A.I. Coppola, S. Wagner, S.T. Lennartz, M. Seidel, N.D. Ward, T. Dittmar, C. Santín, M.W. Jones, The black carbon cycle and its role in the Earth system, Nat. Rev. Earth Environ. 3 (8) (2022) 516–532.
[25] C.M. Long, M.A. Nascarella, P.A. Valberg, Carbon black vs. black carbon and other airborne materials containing elemental carbon: physical and chemical distinctions, Environ. Pollut. 181 (2013) 271–286.
[26] Y.D. Yücel, E. Adolfsson, H. Dykhoff, J. Pettersson, S. Trey, M. Wysocki, E. Widenkvist Zetterström, D. Zenkert, R. Wreland Lindström, G. Lindbergh, Enhancing structural battery performance: investigating the role of conductive carbon additives in LiFePO4-Impregnated carbon fiber electrodes, Compos. Sci. Technol. 251 (2024) 110571.
[27] X. Lu, G.J. Lian, J. Parker, R. Ge, M.K. Sadan, R.M. Smith, D. Cumming, Effect of carbon blacks on electrical conduction and conductive binder domain of next-generation lithium-ion batteries, J. Power Sources 592 (2024) 233916.
[28] Q. Zhang, Z. Yu, P. Du, C. Su, Carbon nanomaterials used as conductive additives in lithium ion batteries, RECENT PAT NANOTECH 4 (2) (2010) 100–110.
[29] M.-J. Kleefoot, S. Enderle, J. Sandherr, M. Bolsinger, T. Maischik, N. Simon, J. Martan, S. Ruck, V. Knoblauch, H. Riegel, Enhancement of the wettability of graphite-based lithium-ion battery anodes by selective laser surface modification using low energy nanosecond pulses, J. Adv. Manuf. Technol. 118 (5) (2022) 1987–1997.
[30] ASTM-International, Standard Test Method for Oil Absorption of Pigments by Gardner-Coleman Method, ASTM D1483-12, 2012.
[31] S. Duan, M. Cattaruzza, V. Tu, R.M. Auenhammer, R. Jänicke, M.K.G. Johansson, F. Liu, L.E. Asp, Three-dimensional reconstruction and computational analysis of a structural battery composite electrolyte, Commun. Mater. 4 (1) (2023).
[32] M. Cattaruzza, Y. Fang, I. Furó, G. Lindbergh, F. Liu, M. Johansson, Hybrid polymer–liquid lithium ion electrolytes: effect of porosity on the ionic and molecular mobility, J. Mater. Chem. A 11 (13) (2023) 7006–7015.
[33] S. Emilsson, V. Vijayakumar, J. Mindemark, M. Johansson, Exploring the use of oligomeric carbonates as porogens and ion-conductors in phase-separated structural electrolytes for Lithium-ion batteries, Electrochim. Acta 449 (2023).
[34] Q. Shen, L.-H. Jiang, Enhancement of the wettability of carbon blacks by electrocapillary rise wetting, ChemistrySelect 1 (12) (2016) 3132–3135.
[35] X. Guo, Z. Ju, X. Qian, Y. Liu, X. Xu, G. Yu, A stable solid polymer electrolyte for lithium metal battery with electronically conductive fillers, Angew Chem. Int. Ed. Engl. 62 (7) (2023) e202217538.
[36] S. Dubinsky, J.I. Park, I. Gourevich, C. Chan, M. Deetz, E. Kumacheva, Toward controlling the surface morphology of macroporous copolymer particles, Macromol. 42 (6) (2009) 1990–1994.
[37] K. Sakakibara, H. Kagata, N. Ishizuka, T. Sato, Y. Tsujii, Fabrication of surface skinless membranes of epoxy resin-based mesoporous monoliths toward advanced separators for lithium ion batteries, J. Mater. Chem. A 5 (15) (2017) 6866–6873.
[38] M. Cattaruzza, M. Johansson, G. Lindbergh, F. Liu, Hybrid polymer-liquid electrolytes and their interactions with electrode materials, Chemelectrochem (2025) e202400561 n/a (n/a).